CrystEngComm

COMMUNICATION

View Article Online
View Journal | View Issue

Cite this: *CrystEngComm*, 2014, **16**, 8317

Received 30th April 2014,
Accepted 17th June 2014

DOI: 10.1039/c4ce00916a

www.rsc.org/crystengcomm

Facile synthesis of hollow Ag@AgBr heterostructures with highly efficient visible-light photocatalytic properties†

Qingsong Dong,[a] Zhengbo Jiao,[a] Hongchao Yu,[a] Jinhua Ye[b] and Yingpu Bi*[a]

A hollow Ag@AgBr photocatalyst was obtained by a replacement reaction between Br^- ions and solid Ag_2CrO_4 and a subsequent light-induced chemical reduction reaction. The photocatalyst exhibits very high photocatalytic activity for the degradation of organic contaminants under visible-light irradiation.

Semiconductor photocatalysis has become a promising approach for resolving current environmental and energy problems by utilizing solar light. However, the photo-catalytic efficiencies of these catalysts are greatly influenced by their intrinsic chemical and physical properties. For example, anatase (TiO_2) has been extensively studied as a photocatalyst for various reactions due to its low cost, strong oxidizing power and nontoxic nature.[1–3] However, its large band gap of 3.2 eV means that it is only excited by UV irradiation (only 4% of the total sunlight), which greatly limits its efficiency in the utilization of solar energy and therefore its practical applications. Therefore, great effort has been devoted to the exploration and preparation of novel semiconductor photo-catalysts with highly efficient visible-light-driven performances.[4–7] Recently, it has been found that the rational design and construction of plasmonic photo-catalysts, composed of noble-metal nanoparticles (NPs) and semiconductor catalysts is one of the most promising approaches for improving photocatalytic performance, as a result of the strong visible-light absorption of noble-metal NPs.[8–16] Moreover, when their interfaces are well controlled, the efficiency of charge separation and transport in these photocatalysts will be greatly improved. Furthermore, it has been reported that the photocatalytic efficiency of plasmonic photocatalysts can be further enhanced by fabricating hollow structures.[17] Because both the surface and interior of hollow structure are accessible, a better distribution of noble-metal NPs can be achieved. The strong surface plasmonic resonance (SPR) absorption of visible light and multi-reflection in the cavity can increase the photocatalytic total absorption efficiency of photon energies.[18] In addition, hollow semiconductors are lightweight and tend to disperse homogeneously in photocatalytic reaction systems. So, hollow nanostructures that consist of plasmonic noble-metal NPs should greatly improve the performance of photocatalysts.

As is known, AgBr can be partially converted *in situ* to plasmonic silver NPs, and their interfaces can be clean and well-defined. These properties have recently been utilized in the design and fabrication of photocatalytic systems, and the results show that differently shaped AgBr or Ag@AgBr hybrids could serve as highly stable and active visible-light-driven photocatalysts for the degradation of organic pollutants[11,19–23] and the conversion of CO_2 to organic compounds.[24] However, a hollow AgBr or Ag@AgBr nanostructure has not yet been reported, and its photocatalytic activity is unknown. Thus, it is highly desirable to explore facile and efficient methods for the large-scale fabrication of high quality hollow Ag@AgBr nanostructures to further improve their photocatalytic performance.

Herein, we demonstrate a simple and powerful strategy for the fabrication of a highly efficient and stable visible-light Ag@AgBr photocatalyst with well-defined hollow interiors through sacrificial template synthesis and a sunlight-induced chemical reduction process. Because of the strong visible light absorption of the Ag^0 species that coexists in the AgBr nanorods and the large surface area of the hollow nanostructures, the as-prepared Ag@AgBr hollow nanostructures exhibited much higher photocatalytic activity than solid Ag@AgBr nanoparticles and Ag@AgBr microrods for decomposing organic pollutants (rhodamine B) under visible-light illumination.

One-dimensional Ag_2CrO_4 nanorods have been obtained by the precipitation reaction between $[Ag(NH_3)_2]\cdot NO_3$ and

[a] *State Key Laboratory for Oxo-Synthesis & Selective Oxidation, and National Engineering Research Center for Fine Petrochemical Intermediate, Lanzhou Institute of Chemical Physics CAS, Lanzhou, 730000, China. E-mail: yingpubi@licp.cas.cn*

[b] *Research Unit for Environmental Remediation Materials, National Institute for Materials Science (NIMS), Tsukuba, 305-0047, Japan*

† Electronic supplementary information (ESI) available: Experimental procedure and additional figures. See DOI: 10.1039/c4ce00916a

$K_2Cr_2O_7$ in aqueous solution, which serve as the starting template as well as the silver ion source for the subsequent fabrication of hollow AgBr nanostructures. Fig. 1A presents a typical scanning electron microscopy (SEM) image of the as-obtained Ag_2CrO_4 nanorods and clearly shows that the Ag_2CrO_4 nanorods have an average diameter of 300 nm and a length of 1 μm. Fig. 1B shows a SEM image of the AgBr nanoproducts which were prepared by mixing the Ag_2CrO_4 nanorods with NaBr in an aqueous PVP solution at room temperature. It can be clearly seen that large quantities of the hollow AgBr nanostructure with a morphology similar to the Ag_2CrO_4 precursor have been synthesized by a simple replacement process, and the thickness of the AgBr shell is estimated to be about 40–50 nm. Moreover, their EDS result (Fig. S1†) shows that only Ag and Br are present in the EDS pattern and no Cr is detected in the final sample, indicating that the Ag_2CrO_4 nanorods have been completely converted into hollow AgBr nanoframes after the controlled anion-exchange reaction. Furthermore, note that the morphologies of the AgBr nanoproducts were determined by the speed at which the Br^- ions were added. As shown in Fig. S2,† with increased adding speed only irregular AgBr nanoparticles were formed, and no hollow structures were observed. When hollow AgBr nanorods were dispersed into deionized water and irradiated under sunlight some Ag^+ ions are reduced to Ag^0, along with a color change from light yellow to gray. In the light reduction process, the resulting Ag atoms may distribute on both the surface and the interior of the hollow AgBr nanorods, which makes the surface appear rough, as shown in Fig. 1C. The geometry and hollow interior of the as-prepared Ag@AgBr nanoframes have also been further confirmed by transmission electron microscopy (TEM). The TEM image in Fig. 1D shows the hollow rod-like structure of the as-prepared Ag@AgBr heterostructures.

Furthermore, the crystalline structure and UV-Vis absorption of the hollow AgBr and Ag@AgBr nanorods have been examined, and are shown in Fig. 2. Compared with the X-ray diffraction (XRD) pattern of pure Ag_2CrO_4 nanorods shown in Fig. S3,† the XRD pattern of the AgBr nanoproducts after the ion-exchange process (Fig. 2A) clearly indicates that all of the diffraction peaks could be assigned to diffraction from the (111), (200), (220), (222), (400), (420), and (422) planes of AgBr crystals (PCPDF no. 06-0438), revealing that the Ag_2CrO_4 nanorods have been completely converted to AgBr products. In this anion-exchange process, the Cr atoms are always in the form of CrO_4^{2-}, the CrO_4^{2-} ions in the Ag_2CrO_4 nanorod precursor are replaced by Br^- ions and exist in the form of free CrO_4^{2-} ions, which can be proved by the XRD pattern of the product, as shown in Fig. S4,† obtained from the supernatant fluid of the reaction. However, in the case of Ag@AgBr hollow nanorods, no obvious metallic silver peaks are observed after irradiation with sunlight, which may be due to the low concentration and small crystalline size of the Ag domains in the product. Fig. 2B shows the UV-Vis absorption spectra of the as-synthesized hollow AgBr and Ag@AgBr nanorods. It can be clearly seen that the hollow AgBr nanorods only show strong absorption in the ultraviolet region with an absorption edge at 450 nm. Compared to its precursor, Ag@AgBr exhibits a stronger absorption in both the ultraviolet and visible regions due to the contribution of the SPR of the silver NPs. These results clearly show that the *in situ* photodeposition of Ag nanocrystals on the surfaces of AgBr nanorods could greatly enhance their visible light absorption. In order to further investigate its composition and clarify the existence of metallic Ag NPs in the sample, X-ray photoelectron spectroscopy (XPS) analysis was performed. The full XPS spectrum confirms the existence of Ag and Br elements (Fig. S5† and Fig. 2C–D). More

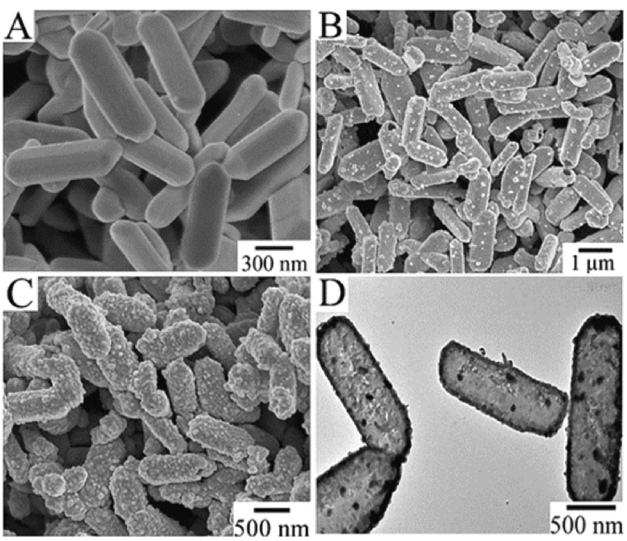

Fig. 1 SEM images of A) Ag_2CrO_4 nanorods, B) hollow AgBr nanorods, and C) hollow Ag@AgBr nanorods; D) TEM image of the hollow Ag@AgBr nanorods.

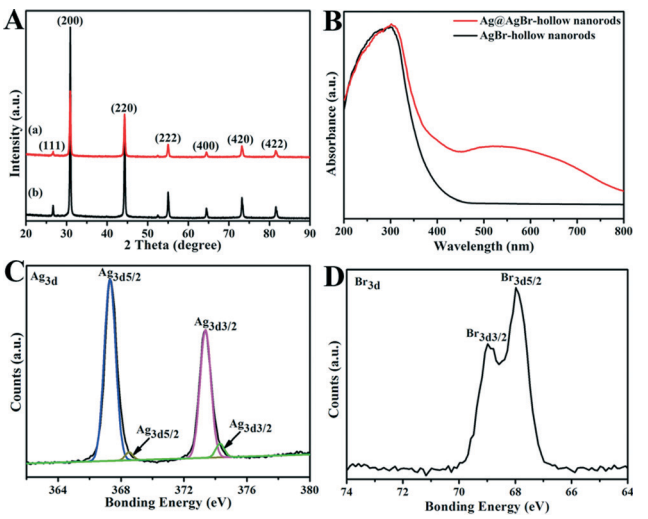

Fig. 2 A) XRD patterns of the hollow AgBr nanorods and the as-prepared hollow Ag@AgBr nanorods; B) UV-Vis absorption spectra of the hollow AgBr nanorods and the hollow Ag@AgBr nanorods; C) Ag 3d peaks, survey scan; D) Br 3d peaks. The fitting reveals the existence of a small portion of Ag^0 in the as-synthesized nanoframes.

specifically, the Ag $3d_{5/2}$ and Ag $3d_{3/2}$ peaks appeared at binding energies of 367.3 eV and 373.3 eV (Fig. 2C), respectively, and the splitting of the 3d doublet was 6.0 eV, which clearly reveals the metallic nature of the silver, demonstrating that Ag NPs had been successfully deposited onto the surfaces of the AgBr nanorods.

During the hollowing process of the AgBr nanorods, the reaction solutions were quenched at various time intervals to study their possible growth mechanism. Fig. 3 shows typical SEM and TEM images corresponding to the morphological and structural evolution involved in this novel AgBr nanorod growth process. As shown in Fig. 3A, these Ag_2CrO_4 nanorods possess relatively smooth and clean surfaces before the anion-exchange reactions. Once the anion-exchange reaction between Br^- ions and solid Ag_2CrO_4 nanostructures occurred, uniform AgBr nanocrystals formed tidily on the surfaces of the Ag_2CrO_4 nanorods to make the surface appear rough (Fig. 3B). However, upon further increasing the reaction time from 5 min to 20 min (Fig. 3B–E), it is difficult to distinguish the degree of reactions from the surface of products, so TEM images are also shown in the insets of Fig. 3A–E. It can be clearly seen that the reaction was initiated first on the surface and then in the interior at both ends of the template Ag_2CrO_4 nanorods (the inset of Fig. 3B), thus implying that the reaction was initiated locally rather than uniformly over the entire nanorods. Over the next 5 min, the interior of the nanorod gradually becomes empty to form a hollow rod with relatively thick walls (the inset of Fig. 3C). After another 5 min the void was further increased in size with relatively thin walls (the inset of Fig. 3D), note that the Ag_2CrO_4 in the interior had not completely disappeared. Therefore, an extended time is needed to ensure the complete conversion of solid Ag_2CrO_4 nanorods to hollow AgBr nanorods. The inset of Fig. 3E shows that nanorods became completely empty at 20 min. Moreover, the UV-Vis spectra of the products formed at different reaction times were also measured and are shown in Fig. 3F. As the anion-exchange reaction is prolonged, the characteristic absorption peak of Ag_2CrO_4 at 400 nm is reduced very quickly. The absorption peak intensity of AgBr increases with increasing reaction time, which indicates the continuous formation of AgBr. Finally, only the diffraction peaks of AgBr crystals were observed after the replacement process due to the complete conversion to AgBr. Furthermore, the XRD patterns of the products formed at different reaction times were also studied (Fig. S3†). It can be clearly seen that the diffraction peaks of Ag_2CrO_4 were gradually reduced during the ion-exchange process, and the peaks of AgBr were significantly enhanced. Additionally, except for the Ag_2CrO_4 and AgBr, no diffraction peaks corresponding to other impurities are detected, indicating that the obtained hollow structures in the whole growth process only consisted of Ag_2CrO_4 and AgBr crystals, and their compositions can be easily adjusted.

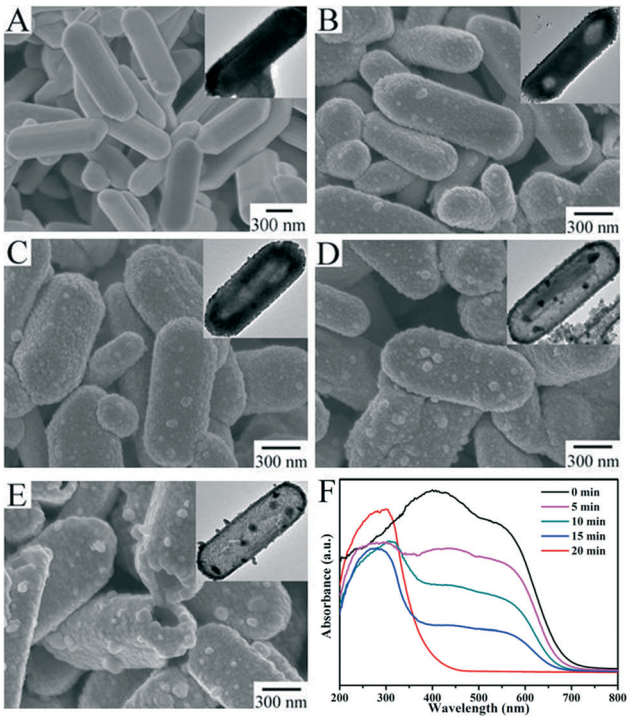

Fig. 3 SEM images of hollow AgBr nanorods during the growth process at different reaction times: A) 0, B) 5, C) 10, D) 15, E) 20 min (insets show the TEM images of the products at the corresponding reaction times, scale bar = 300 nm), and F) their corresponding UV-Vis spectra.

For the Ag@AgBr hollowing process, compared with the system under acidic conditions,[13] the ion-exchange reaction is more easily controlled under neutral conditions, and thus a hollow structure with morphology similar to that of the template can be obtained. On the basis of the above result, we identified a potential reaction route explaining the above hollowing process, and a schematic illustration is shown in Scheme 1. In the presence of NaBr, the ion-exchange reaction of Ag_2CrO_4 with Br^- ions was initiated first on the surface of Ag_2CrO_4 nanorod, resulting in a layer of AgBr. With a continuous supply of Br^- ions for the exchange reaction, the reaction proceeded in the interior at both ends of the template Ag_2CrO_4 nanorod. As the mobility of Ag^+ cations is much higher than that of Br^- ions in the forming cavity, the Ag^+ ions spread to the outside to react with Br^-, forming AgBr at the peripheral surfaces of the nanorod owing to the known nanoscale Kirkendall effect.[25,26] Meanwhile, when the concentration of Br^- ions is too high, Br^- ions will quickly

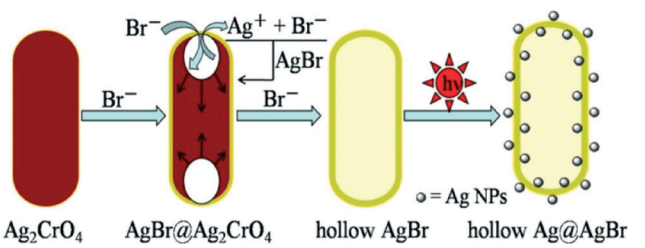

Scheme 1 Illustration of the transformation of the Ag_2CrO_4 nanorods into hollow Ag@AgBr nanoframes through the anion-exchange Kirkendall effect and sunlight-induced chemical reduction reaction.

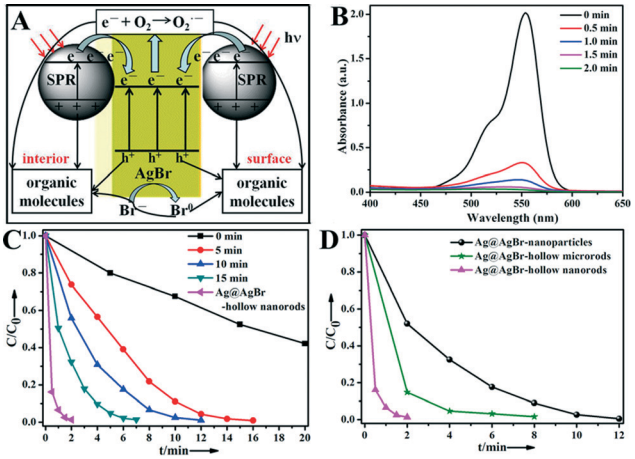

Fig. 4 A) Photocatalytic reaction process and charge transfer of the hollow Ag@AgBr heterostructures under visible-light irradiation; B) the variation in the absorption of the RhB dye over the hollow Ag@AgBr nanorods at different irradiation times; C) photodegradation of RhB dye over the as-prepared hollow Ag@AgBr nanorods and the intermediate products at different reaction times: 0, 5, 10, and 15 min under visible light; D) photocatalytic activity of Ag@AgBr samples: hollow Ag@AgBr nanorods, hollow Ag@AgBr microrods and Ag@AgBr nanoparticles for the degradation of RhB dye under visible light irradiation.

react with Ag^+ spreading from the cavity to form AgBr nanoparticles at the cavity and not the peripheral surfaces of the nanorod, resulting in the collapse of the layer of AgBr. Finally, AgBr particles generate an electron–hole pair upon absorbing a photon, and the photogenerated electron combines with an Ag^+ ion to form an Ag^0 atom. A layer of Ag^0 atoms forms on both the surface and interior of the hollow AgBr rod upon repeated absorption of photons, yielding a hollow Ag@AgBr nanorod.

Finally, the possible photocatalytic mechanism induced by visible-light responsive hollow Ag@AgBr is shown in Fig. 4A. Electrons and holes could be generated from the photoexcited AgBr shell under visible-light irradiation. Due to the dipolar character of the SPR effect of both the surface and interior Ag NPs, the electrons generated from the plasmon-excited Ag NPs could migrate to the conduction band (CB) of AgBr, where they can be trapped by O_2 in solution to form $O_2^{\cdot -}$,[27] which are reactive species responsible for the destruction of organic molecules. Concomitantly, the photoproduced holes in the valence band (VB) of AgBr could oxidize Br^- to Br^0, which could oxidize organic molecules while being reduced to Br^-; the remaining positive charge on the Ag NPs can also contribute to the oxidation of organic dyes.[28] Furthermore, the photocatalytic activity of the as-prepared Ag@AgBr hollow nanoframe was investigated by the degradation of Rhodamine B (RhB) under visible light (Fig. 4B), and it can nearly completely decompose 100 mL 10 mg L^{-1} RhB within 2 min of visible-light irradiation. To study the influence of the degree of reaction on the catalytic performance, the hollow nanorods formed at different reaction times were also used as catalysts. As can be seen in Fig. 4C, the catalytic performance was improved with the increase of reaction degree, and the hollow Ag@AgBr nanorods (product of 100% reaction) showed the best photocatalytic properties. Moreover, the performances of the Ag@AgBr nanoparticles and the hollow Ag@AgBr microframe have also been investigated and are compared in Fig. 4D. It can be clearly seen that the complete degradation of RhB dye over the hollow microrod sample (SEM image in Fig. S6A†) takes about 8 min, while the nanoparticle sample (SEM image in Fig. S6B†) takes about 12 min. These results clearly indicate that the morphology-controlled synthesis of the catalyst is a very effective strategy for enhancing the photocatalytic performance.

In addition to the photocatalytic efficiency, the stability of the photocatalyst is also an important factor for potential applications, so cyclic bleaching experiments of the Ag@AgBr hollow nanorods for RhB were carried out. The photocatalyst was collected by centrifugation and used to catalyze new reactions for four cycles, and the photocatalytic performance is shown in Fig. S7,† which indicates that the recycled catalysts show a significant decrease in their degradation rate after three additional cycles. The XRD result in Fig. S8† reveals that the sample of hollow Ag@AgBr nanorods possessed a similar composition to the as-prepared sample after every cycle. However, the SEM image (Fig. S9†) shows that the hollow morphology of the as-prepared sample was slowly collapsing, which may result in a decrease in their degradation rate.

Conclusions

We have demonstrated a facile and efficient strategy for fabricating hollow Ag@AgBr nanoframes through a controlled anion-exchange reaction and a subsequent sunlight-induced chemical reduction reaction. Moreover, the photocatalytic performance studies indicate that the hollow Ag@AgBr nanoframe exhibited much higher activity than its nanoparticle and hollow microframe counterparts for organic contaminant degradation under visible-light irradiation. Finally, these demonstrations clearly reveal that the rational fabrication of a hollow plasmonic semiconductor nanostructure may be an effective technique for the development of highly efficient visible-light sensitive photocatalysts.

Acknowledgements

This research was supported by the "Hundred Talents Program" of the Chinese Academy of Science, and National Natural Science Foundation of China (21273255, 21303232). The authors deeply appreciate the support.

Notes and references

1 M. Hoffmann, S. Martin, W. Choi and D. Bahnemann, *Chem. Rev.*, 1995, **95**, 69.
2 G. Brown, V. Henrich, W. Casey, D. Clark, C. Eggleston, A. Femly, D. Goodman, M. Gratzel, G. Macial, M. McGarthy, K. Nealson, D. Sverjensky, M. Toney and J. Zachara, *Chem. Rev.*, 1999, **99**, 77.

3 W. Yao, X. Xu, H. Wang, J. Zhou, X. Yang, Y. Zhang, S. Shang and B. Huang, *Appl. Catal., B*, 2004, **52**, 109.
4 A. Linsebigler, G. Lu and J. Yates Jr., *Chem. Rev.*, 1995, **95**, 735.
5 S. Livraghi, A. Votta, M. Paganini and E. Giamello, *Chem. Commun.*, 2005, 498.
6 B. Kale, J. Baeg, S. Lee, H. Chang, S. Moon and C. Lee, *Adv. Funct. Mater.*, 2006, **16**, 1349.
7 K. Yang, Y. Dai, B. Huang and M. Whangbo, *Chem. Mater.*, 2008, **20**, 6528.
8 K. Awazu, M. Fujimaki, C. Rockstuhl, J. Tominaga, H. Murakami, Y. Ohki, N. Yoshida and T. Watanabe, *J. Am. Chem. Soc.*, 2008, **130**, 1676.
9 X. Chen, H. Zhu, J. Zhao, Z. Zheng and X. Gao, *Angew. Chem., Int. Ed.*, 2008, **47**, 5353.
10 P. Wang, B. Huang, X. Qin, X. Zhang, Y. Dai, J. Wei and M. Whangbo, *Angew. Chem., Int. Ed.*, 2008, **47**, 7931.
11 P. Wang, B. Huang, X. Zhang, X. Qin, H. Jin, Y. Dai, Z. Wang, J. Wei, J. Zhan, S. Wang, J. Wang and M. Whangbo, *Chem. – Eur. J.*, 2009, **15**, 1821.
12 W. Wang, W. Lu and L. Jiang, *J. Colloid Interface Sci.*, 2009, **338**, 270.
13 L. Kuai, B. Geng, X. Chen, Y. Zhao and Y. Luo, *Langmuir*, 2010, **26**, 18723.
14 P. Wang, B. Huang, Z. Lou, X. Zhang, X. Qin, Y. Dai, Z. Zheng and X. Wang, *Chem. – Eur. J.*, 2010, **16**, 538.
15 C. An, S. Peng and Y. Sun, *Adv. Mater.*, 2010, **22**, 2570.
16 C. An, J. Wang, J. Liu, S. Wang and Y. Sun, *ChemSusChem*, 2013, **6**, 1931.
17 X. Cao, L. Gu, L. Zhuge, W. Gao, W. Wang and S. Wu, *Adv. Funct. Mater.*, 2006, **16**, 896.
18 Y. Tang, Z. Jiang, G. Xing, A. Li, P. Kanhere, Y. Zhang, T. Sum, S. Li, X. Chen, Z. Dong and Z. Chen, *Adv. Funct. Mater.*, 2013, **23**, 2932.
19 G. Li, K. Wonga, X. Zhang, C. Hu, J. Yu, R. Chan and P. Wong, *Chemosphere*, 2009, **76**, 1185.
20 Y. Bi and J. Ye, *Chem. – Eur. J.*, 2010, **16**, 10327.
21 H. Wang, J. Gao, T. Guo, R. Wang, L. Guo, Y. Liuc and J. Li, *Chem. Commun.*, 2012, **48**, 275.
22 C. Hu, Y. Lan, J. Qu, X. Hu and A. Wang, *J. Phys. Chem. B*, 2006, **110**, 4066.
23 H. Wang, J. Yang, X. Li, H. Zhang, J. Li and L. Guo, *Small*, 2012, **8**, 2802.
24 C. An, J. Wang, W. Jiang, M. Zhang, X. Ming, S. Wanga and Q. Zhang, *Nanoscale*, 2012, **4**, 5646.
25 Y. Yin, R. Rioux, C. Erdonmez, S. Hughes, G. Somorjai and A. Alivisatos, *Science*, 2004, **304**, 711.
26 E. Gonzlez, J. Arbiol and V. Puntes, *Science*, 2011, **334**, 1377–1380.
27 S. Soni, M. Henderson, J. Bardeau and A. Gibaud, *Adv. Mater.*, 2008, **20**, 1493.
28 X. Zhou, C. Hu, X. Hu, T. Peng and J. Qu, *J. Phys. Chem. C*, 2010, **114**, 2746.